A Phase Separation Model for the Nanopatterning of Diatom Biosilica

Manfred Sumper

Science **295**, 2430 (2002);
DOI: 10.1126/science.1070026

to be again logarithmically accurate, not fundamentally different in this respect from CA. We therefore expect that a quantum computation based on QA will not transform a hard nonpolynomial (NP-complete) computational problem into a polynomial one. On the contrary, the above reasoning suggests that a logarithmically slow annealing also applies to the present 2D Ising case, which is not NP-complete (*14*). The slowing-down effect of the LZ cascade illustrated above is particularly severe in problems, like the Ising spin glass we have considered, where the classical spectrum has a gapless continuum of excitations above the ground state. Satisfiability problems, for which encouraging results were recently presented (*10*), differ from the Ising spin glass in that they possess a discrete classical spectrum and a finite excitation gap. We observe that in general a gap will cut off the LZ cascade precisely in the dangerous low-Γ region, which may eliminate the logarithmic slowing down of QA. Nonetheless, even in the gapless case, the advantage of QA over CA is far from negligible because of the generally larger exponent ζ_{QA} of the logarithm. To get an idea of the order of magnitudes involved, consider the relative increase of annealing time (τ'/τ) needed to improve the accuracy of a certain annealing, say with $\tau \approx 10^6$ (in appropriate units), by a factor of 10. In CA ($\zeta = 2$), this would require $(\tau'/\tau) \approx \tau^{[10^{(1/\zeta)}]-1} \approx 10^{13}$. In QA ($\zeta = 6$), the same result would be accomplished with $(\tau'/\tau) \approx 10^{2.8}$, an enormous saving of computer effort. Moreover, the PIMC version of QA is easy to implement on a parallel computer, which provides an extra advantage. Optimization by QA of a vast variety of problems, after a suitable fictitious kinetic term is identified case by case, is an open avenue and stands as a worthy challenge for the future.

References and Notes

1. S. Kirkpatrick, C. D. Gelatt Jr., M. P. Vecchi, *Science* **220**, 671 (1983).
2. V. Černý, *J. Opt. Theor. Appl.* **45**, 41 (1985).
3. D. A. Huse, D. S. Fisher, *Phys. Rev. Lett.* **57**, 2203 (1986).
4. J. Brooke, D. Bitko, T. F. Rosenbaum, G. Aeppli, *Science* **284**, 779 (1999).
5. J. Brooke, T. F. Rosenbaum, G. Aeppli, *Nature* **413**, 610 (2001).
6. A. B. Finnila, M. A. Gomez, C. Sebenik, C. Stenson, J. D. Doll, *Chem. Phys. Lett.* **219**, 343 (1994).
7. T. Kadowaki, H. Nishimori, *Phys. Rev. E* **58**, 5355 (1998).
8. Y. H. Lee, B. J. Berne, *J. Phys. Chem. A* **104**, 86 (2000).
9. ———, *J. Phys. Chem. A* **105**, 459 (2001).
10. E. Farhi *et al.*, *Science* **292**, 472 (2001).
11. G. S. Grest, C. M. Soukoulis, K. Levin, *Phys. Rev. Lett.* **56**, 1148 (1986).
12. A. Chakrabarti, R. Toral, *Phys. Rev. B* **39**, 542 (1989).
13. P. Ocampo-Alfaro, H. Guo, *Phys. Rev. B* **53**, 1982 (1996).
14. F. Barahona, *J. Phys. A* **15**, 3241 (1982).
15. For each set of couplings, E_{GS} is calculated using the Spin Glass Ground State Server at www.informatik.uni-koeln.de/ls_juenger/projects/sgs.html.
16. D. S. Fisher, D. A. Huse, *Phys. Rev. Lett.* **56**, 1601 (1986).
17. M. Suzuki, *Prog. Theor. Phys.* **56**, 1454 (1976).
18. Supplementary details of the method are available on *Science* Online at www.sciencemag.org/cgi/content/full/295/5564/2427/DC1.
19. E. Lieb, D. Mattis, *J. Math. Phys.* **3**, 749 (1962).
20. H. Rieger, A. P. Young, *Phys. Rev. Lett.* **72**, 4141 (1994).
21. M. J. Thill, D. A. Huse, *Physica A* **214**, 321 (1995).
22. W. Wu, D. Bitko, T. F. Rosenbaum, G. Aeppli, *Phys. Rev. Lett.* **71**, 1919 (1993).
23. L. D. Landau, E. M. Lifshitz, *Quantum Mechanics—Non-Relativistic Theory* (Pergamon, Oxford, 1977).

24. This project was sponsored by the Ministero dell'Istruzione, dell'Università e della Ricerca under project COFIN, by INFM/G, INFM/F, and by INFM's Iniziativa Trasversale Calcolo Parallelo. R.M. acknowledges European Union support through CINECA under project MINOS3, which also provided much of the computer resources. We thank G. Aeppli, L. Arrachea, J. Berg, C. Micheletti, M. Parrinello, F. Ricci Tersenghi, and R. Zecchina for helpful discussions and suggestions.

7 December 2001; accepted 25 February 2002

A Phase Separation Model for the Nanopatterning of Diatom Biosilica

Manfred Sumper*

Diatoms are encased in an intricately patterned wall that consists of amorphous silica. Species-specific fabrication of this ornate biomineral enables taxonomists to identify thousands of diatom species. The molecular mechanisms that control this nanofabrication and generate the diversity of patterns is not well understood. A simple model is described, in which repeated phase separation events during wall biogenesis are assumed to produce self-similar silica patterns in smaller and smaller scales. On the basis of this single assumption, the apparently complex patterns found in the valves of the diatom genus *Coscinodiscus* can be predicted. Microscopic analysis of valves in statu nascendi from three different *Coscinodiscus* species supports the conclusions derived from the model.

Coscinodiscus is regarded as one of the largest genera of marine planktonic diatoms (*1*). The species *Coscinodiscus asteromphalus*, *Coscinodiscus granii*, *Coscinodiscus radiatus*, and *Coscinodiscus wailesii* are frequently found in marine habitats and can be grown in quantities sufficient for biochemical studies (*2*, *3*). Their siliceous cell wall (valve) (Fig. 1A) is a honeycomb consisting of the vertical areolae walls arranged in hexagons (Fig. 1B). Both the roof and the floor of the honeycomb are formed by plates with numerous perforations. The internal plate exhibits a single hole (foramen) exactly in the center of each hexagon. The outside plate is a thin silica layer (cribrum) perforated by a complex but highly symmetric arrangement of pores. The valve structure can be interpreted as a hierarchy of self-similar patterns. Each of the hexagonally arranged chambers (areolae) embodies a set of hexagonally arranged pores (cribrum), and each of these pores in turn embodies a set of even smaller pores in a hexagonal arrangement (cribellum). It is this elaborate patterning that produces the intricate structures observed under the scanning electron microscope (SEM) (Fig. 1C).

The silica shell of diatoms consists of two overlapping valves (Fig. 1A). During cell division, a new valve is formed inside the cell by controlled precipitation of silica within a specialized membrane vesicle called the silica deposition vesicle (SDV) (*4*). Detailed electron microscopic studies by Schmid and Volcani (*5*) led to a phenomenological description of wall morphogenesis in *C. wailesii*. According to this work, definite stages of silica deposition within the SDV can be discerned during morphogenesis of a new valve. Initially, development of the base layer containing the foraminae is followed by the construction of the hexagonally arranged walls of the areolae. The outer layer (cribrum and cribellum) are completed later. A particular feature of outer-layer construction is that fabrication of the cribrum is centripetal in relation to the areolae, that is, fabrication of the cribrum on top of each areola begins at the hexagonally arranged walls and continues toward the middle of each areola. Finally, all the pores within a cribrum are further modified by precipitating silica to establish the cribellum.

A mechanistic model of wall morphogenesis should explain not only the creation of particular patterns but also the growth behavior of cribra and cribella. An earlier model for pattern formation based on electron microscopic observations postulated a complex and highly regulated assembly of different cell organelles and vesicles creating a precisely shaped mold for the expanding SDV and the precipitating silica in it (*6*). However, the cellular mechanism that could control the

Lehrstuhl Biochemie I, Universität Regensburg, 93053 Regensburg, Germany.

*E-mail: manfred.sumper@vkl.uni-regensburg.de

postulated traffic and arrangement of vesicles of different size classes necessary to create the highly complex pattern remains unknown. A completely different approach for explaining certain aspects of pattern formation in diatoms was proposed by Gordon and Drum (*7*). Their model interprets the riblike silica patterns observed in many diatoms as the result of exclusively physicochemical processes. The patterns were thought to result from a diffusion-limited precipitation of silica nanospheres within the SDV. These models were hampered by the lack of knowledge about the biochemistry of silica precipitation in diatoms.

Recently, silica-associated components from several different diatom species were identified that mediate the formation of silica nanospheres in vitro from a silicic acid solution (*8*–*10*). These substances accelerate silicic acid polymerization and coprecipitate with silica. The compounds have been identified as long-chain polyamines attached to putrescine, and polycationic polypeptides termed silaffins. The latter also contain long-chain polyamines attached to ε-amino-groups of lysine residues. When compounds incorporated into silica by three *Coscinodiscus* species (*C. granii*, *C. wailesii*, and *C. asteromphalus*) were extracted by hydrogen fluoride treatment of purified shells, long-chain polyamines were found to predominate, whereas silaffin-related peptides appear to be absent (*11*). The chain-length distribution of *C. granii* polyamines centers at about 16 propylamine units, whereas that of *C. wailesii* exhibits its maximum at 19 propylamine units. This species specificity of chain-length distribution might indicate a role of the polyamines in the process of biosilica nanopatterning.

Here, a model is proposed that unifies biochemical data and observations obtained by high-resolution SEM. It is postulated that long-chain polyamines not only promote silica precipitation but also are involved in pattern formation. Methylated, long-chain polyamines exhibit amphiphilic properties as indicated by their quantitative extraction from an aqueous solution with chloroform/methanol (*11*). Recent developments in the chemical synthesis of ordered inorganic solids make use of amphiphiles to promote the formation of ordered structures in the nm range by means of liquid-crystal templating (*12*–*15*). The importance of phase transitions during the production of mesoporous silica structures has been recognized (*16*). In the μm range, templating by emulsion droplets has been shown to guide the production of ordered macroporous materials (*17*–*19*). Therefore, the model postulates the existence of repeated phase separation processes within the SDV, which produce emulsions of microdroplets and, subsequently, of nanodroplets or micelles consisting of a polyamine-containing organic phase. As shown here, this postulate is able to predict all the patterns and the growth behavior observed during different stages of wall morphogenesis (Fig. 2).

First, to allow closest packing, the organic droplets become hexagonally arranged in a monolayer within the flat SDV vesicle. The contact sites between polyamine droplets and the aqueous phase that contains the hydrophilic silicic acid promote silicic acid polymerization (Fig. 2A). Precipitating silica necessarily creates a honeycomb-like framework. The holes (foraminae) in this basal silica framework are likely to originate from the contact sites between droplets and the SDV membrane that excludes the aqueous phase.

Second, silica formation consumes a defined fraction of the polyamine population by coprecipitation (*8*, *9*). This fact is assumed to cause a dispersion of the original organic droplets, segregating smaller droplets (Fig. 2B). Guided by the newly created water/polyamine interfaces, silicic acid continues to polymerize and precipitate, thereby consuming another fraction of the polyamine population. This in turn causes the remaining part of the original organic droplet to break up into a maximum number of smaller droplets, again creating new interfaces for silica deposition (Fig. 2C). This scenario accurately explains the pattern observed in the cribrum of *C. wailesii*. Some cases of imperfection mainly observed at positions along the areolae walls indicate the occasional fusion of adjacent secondary droplets, particularly at these sites.

Finally, the creation of the self-similar pattern of the cribellum appears to follow the same

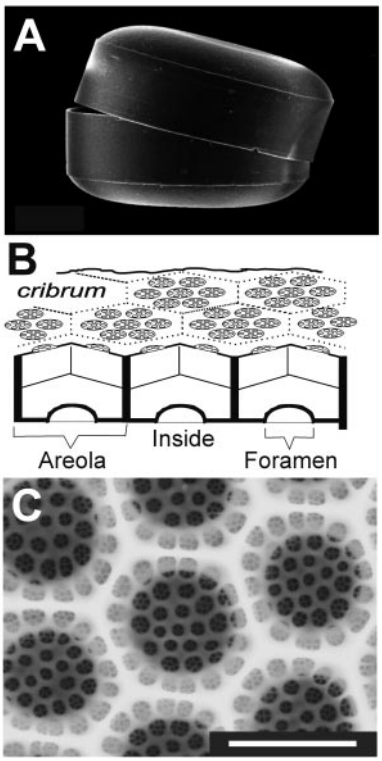

Fig. 1. The form and microarchitecture of the silicified valve from the diatom genus *Coscinodiscus*. (**A**) Scanning electron micrograph of a silica shell (*Coscinodiscus* sp.). (**B**) Diagram of the three-dimensional architecture of the valve. The honeycomb-like chambers are denoted as areolae. The roof on top of each areola is called a cribrum, which contains a regular pattern of larger pores. The siliceous fine structure within each larger pore of a cribrum is denoted as cribellum. (**C**) High-resolution SEM of a valve (areolae, cribra, and cribella) from *C. radiatus*. Bar, 2.5 μm.

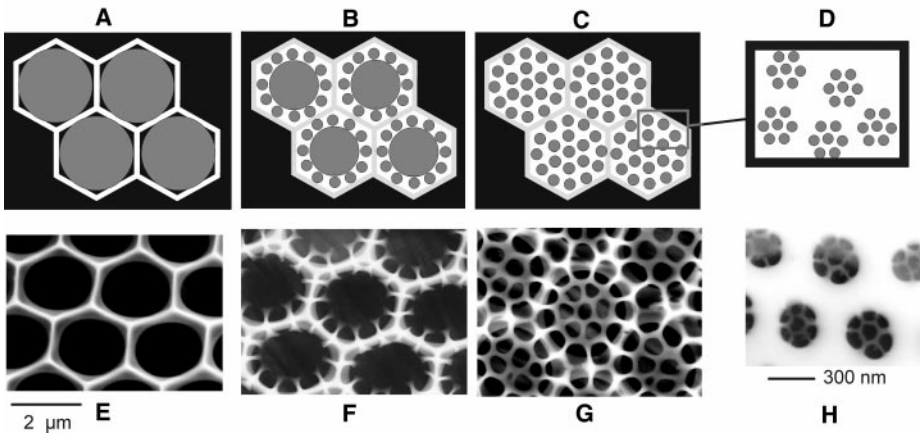

Fig. 2. Schematic drawing of the templating mechanism by the phase separation model [(A) to (D)] and scanning electron micrographs of *C. wailesii* valves in statu nascendi [(E) to (H)]. (**A**) The monolayer of polyamine-containing droplets in close-packed arrangement within the SDV guides silica deposition. (**B** and **C**) Consecutive segregations of smaller (about 300 nm) droplets open new routes for silica precipitation. (**D**) Dispersion of 300-nm droplets into 50-nm droplets guides the final stage of silica deposition. Silica precipitation occurs only within the water phase (white areas). The repeated phase separations produce a hierarchy of self-similar patterns. (**E** to **H**) SEM images of valves in statu nascendi at the corresponding stages of development.

principle. The secondary droplets break up into even smaller droplets (about 50 nm in diameter), again forming a hexagonal package (the pattern shown in Fig. 2D often predominates in *Coscinodiscus* cribella) that guides the final stage of silica deposition. This final round of silica precipitation is assumed to consume all of the remaining polyamine, thereby terminating the process of pattern formation. High-resolution SEM images (Fig. 2, E to H) obtained from the corresponding stages of valve morphogenesis in *C. wailesii* (*20*) confirm the expected growth behavior.

The forces that drive fragmentation of the droplets into smaller and smaller subunits could result from both the consumption of polyamines during precipitation and the concomitant creation of silica surfaces (negatively charged) with a high affinity for a polyamine-containing surface (positively charged). Both these events should favor a surface expansion by fragmentation of the polyamine-containing phase (Fig. 3). If so, it is the expanding growth zone of silica that induces the fragmentation of polyamine-containing droplets, thereby creating new routes for further silica deposition. The silica growth zone is expected to expand into the aqueous phase separating polyamine droplets because these areas should provide the highest concentration of polysilicic acid (only polyamine surfaces accelerate silicic acid polymerization).

This phase separation model is also able to predict the distinct patterns found in the valves from *C. granii* and *C. asteromphalus*. According to the model, the only parameter that dictates the species-specific pattern is the wall-to-wall distance of the areolae, which in our strains is about 0.9 μm in *C. granii*, about 2.0 μm in *C. wailesii*, and about 3.0 μm in *C. asteromphalus*. In the interpretation given by the model, this specificity reflects different sizes of microdroplets produced during the very first event of phase separation. If all subsequent steps follow exactly the scenario described above, the predicted patterns match the observations. Species-specific patterns are the result of the constraints introduced by different wall-to-wall distances within the areolae, which dictate the maximum number and arrangement of the secondary droplets producing the cribrum (Fig. 4). The very short wall-to-wall distance in *C. granii* interferes with the segregation of secondary droplets. Consequently, these droplets appear to be positioned even across an areola wall.

The phase separation processes outlined above were assumed to take place in a static space. This clearly is a simplification: It is well established that controlled and rapid expansion of the SDV occurs during valve morphogenesis. Therefore, it is unrealistic to expect the static model to explain all details of the silicification process. The model can explain the complex patterns produced during formation of the cribrum and cribellum, but other aspects of valve morphogenesis such as the transition from silica deposition in the base layer to silica deposition producing the hexagonal areolae walls can only be explained if a controlled expansion of the SDV with respect to the *z* axis is introduced. In addition, viscoelastic effects can come into play for a dynamic process of phase separation, and this in turn can influence pattern formation (*21*). The silicified strands radiating outward from the valve center during the very first stage of silica deposition might reflect such a viscoelastic behavior of phase separation.

Transmission electron micrographs obtained from diatom cells appear to conflict with the scenario outlined above, because the SDV is seen as a meshwork perforated by many classes of vesicles (*6*). However, these images were obtained from cells after fixation with glutaraldehyde and subsequent extraction with organic solvents. Polyamines are highly reactive with glutaraldehyde. Consequently, organic droplets containing polyamines are likely to develop cross-linked surface films that finally might produce a variety of vesicle-like structures. More important, cytoplasmic membrane systems tend to become vesiculated by glutaraldehyde fixation, and this is probably the most common and insidious artefact in electron microscopy (*22*). Only very recent developments in electron microscopy (cryofixation, cryomicrotomy, and cryotomography) may turn out to be adequate methods to determine the native shape and environment of the SDV.

It appears highly likely that the diversity of diatom valves is achieved by the combinatorial action of a few basic mechanisms of silica deposition. The mechanism proposed here may be part of such a combinatorial system, given that polyamines and silaffins have been detected in a wide range of diatom genera (*9*). In genera like *Stephanopyxis*, cribrum formation and production of hexagonal chambers appear to be separate processes. Only after production of the cribrum, silica precipitation is again initiated on top of the cribrum structure. In terms of the model, *Stephanopyxis* is likely to use two independent phase separation/precipitation events in series. In a pennate diatom, silica is deposited in elongated microfibrillar strands (*23*), structures that could originate by a simple deposition process, without the need for phase transitions. It is tempting to speculate that the high symmetry found in *Coscinodiscus* valves reflects the relatively simple composition of polyamine components. Producing less symmetric silica structures might require the more complex composition of polyamines and silaffin species found in other diatom genera (*9*).

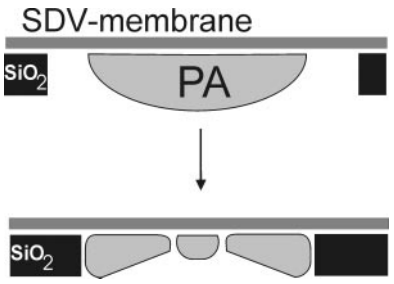

Fig. 3. Hypothetical mechanism of droplet dispersion. The forces that drive fragmentation of polyamine-containing (PA) organic droplets into smaller subunits are suggested to result from both the consumption of polyamines caused by silica precipitation (SiO_2) and the concomitant creation of new silica surfaces (negatively charged) with a high affinity for a polyamine-containing phase (positively charged). This situation should favor a surface expansion by fragmentation of the organic phase. SDV, silica deposition vesicle.

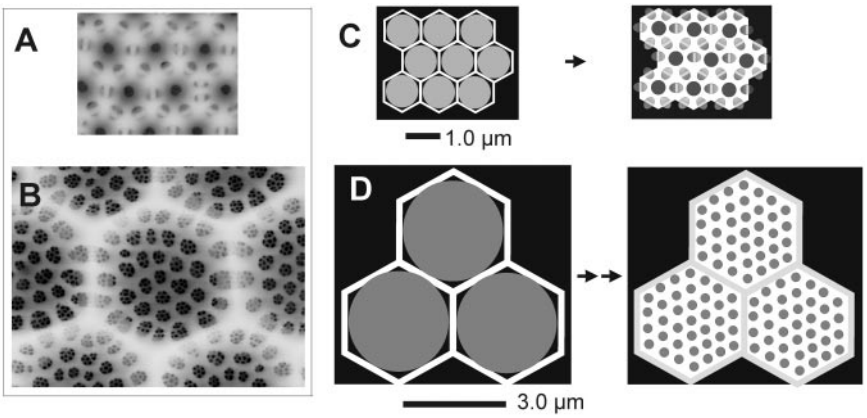

Fig. 4. SEM images of valves from *C. granii* (**A**) and *C. asteromphalus* (**B**) and the interpretation of their patterns by the phase separation model [(**C**) for *C. granii* and (**D**) for *C. asteromphalus*]. The number and arrangement of secondary droplets are governed only by the wall-to-wall distance of the areolae formed during the initial phase of silica precipitation. Only the cribrum pattern formation is shown. The final formation of the self-similar cribellum pattern follows the rules given in Fig. 2D. The wall-to-wall distance in the areolae is about 1 μm in *C. granii* and about 3 μm in *C. asteromphalus*.

References and Notes

1. G. R. Hasle, C. B. Lange, *Diatom Res.* **7**, 37 (1992).
2. C. R. Tomas, *Identifying Marine Phytoplankton* (Academic Press, New York, 1997).
3. *C. granii*, *C. wailesii*, and *C. radiatus* were collected from the North Sea (Germany) and cultivated as axenic unialgal cultures in an artificial seawater medium according to the recipe from the North East Pacific Culture Collection (www.ocgy.ubc.ca/cccm//NEPCC/esaw.html). *C. asteromphalus* was obtained from this culture collection.
4. R. W. Drum, H. S. Pankratz, *J. Ultrastruct. Res.* **10**, 217 (1964).
5. A. M. M. Schmid, B. E. Volcani, *J. Phycol.* **19**, 387 (1983).
6. J. Picket-Heaps, A. M. M. Schmid, L. A. Edgar, in *Progress in Phycological Research*, F. E. Round, D. J. Chapman, Eds. (Biopress, Bristol, UK, 1990), vol. 7, pp. 1–169.
7. R. Gordon, R. W. Drum, *Int. Rev. Cytol.* **150**, 243 (1994).
8. N. Kröger, R. Deutzmann, M. Sumper, *Science* **286**, 1129 (1999).
9. N. Kröger, R. Deutzmann, C. Bergsdorf, M. Sumper, *Proc. Natl. Acad. Sci. U.S.A.* **97**, 14133 (2000).
10. N. Kröger, R. Deutzmann, M. Sumper, *J. Biol. Chem.* **276**, 26066 (2001).
11. A supplementary figure and details of experimental procedures are available on *Science* Online at www.sciencemag.org/cgi/content/full/295/5564/2430/DC1.
12. C. T. Kresge, M. E. Leonowicz, W. J. Roth, J. C. Vartuli, J. S. Beck, *Nature* **359**, 710 (1992)
13. S. Mann, G. A. Ozin, *Nature* **382**, 313 (1996).
14. H. P. Lin, C. Y. Mou, *Science* **273**, 765 (1996).
15. H. Yang, N. Coobs, G. A. Ozin, *Nature* **386**, 692 (1997).
16. A. Monnier *et al.*, *Science* **261**, 1299 (1993).
17. G. Widawski, B. Rawiso, B. Francois, *Nature* **369**, 387 (1994).
18. S. Schacht, Q. Huo, I. G. Voigt-Martin, G. D. Stucky, F. Schüth, *Science* **273**, 768 (1996).
19. A. Imhof, D. J. Pine, *Nature* **389**, 948 (1997).
20. SEM images were obtained on a Leo 1530 field-emission scanning electron microscope. *Coscinodiscus* valves in statu nascendi were obtained from a growing cell culture by treating the harvested cells twice with hot 2% SDS–100 mM EDTA to remove intracellular material, membranes, and wall coatings. Cell walls were pelleted by low-speed centrifugation (1000*g*), washed repeatedly with water, and dried. Inspection for valves in different stages of morphogenesis was done by SEM screening.
21. H. Tanaka, *Phys. Rev. Lett.* **76**, 787 (1996).
22. G. Griffiths, *Fine Structure Immunochemistry* (Springer, New York, 1993).
23. J. D. Pickett-Heaps, D. H. Tippit, J. A. Andreozzi, *Biol. Cell.* **35**, 199 (1979).

24. I thank R. Fischer for technical assistance, E. Hochmuth and R. Deutzmann for mass spectrometry analysis, and W. Tanner for helpful discussions. This work was supported by the Deutsche Forschungsgemeinschaft (SFB 521-A2).

22 January 2002; accepted 21 February 2002

Atomic-Level Observation of Disclination Dipoles in Mechanically Milled, Nanocrystalline Fe

M. Murayama,[1]* J. M. Howe,[1]† H. Hidaka,[2] S. Takaki[2]

Plastic deformation of materials occurs by the motion of defects known as dislocations and disclinations. High-resolution transmission electron microscopy was used to directly reveal the individual dislocations that constitute partial disclination dipoles in nanocrystalline, body-centered cubic iron that had undergone severe plastic deformation by mechanical milling. The mechanisms by which the formation and migration of such partial disclination dipoles during deformation allow crystalline solids to fragment and rotate at the nanometer level are described. Such rearrangements are important basic phenomena that occur during material deformation, and hence, they may be critical in the formation of nanocrystalline metals by mechanical milling and other deformation processes.

Mechanical milling is a technique for producing metallic alloys with ultrafine grain sizes by severe plastic deformation (*1*–*4*). These nanocrystalline alloys have unique mechanical properties, such as hardnesses and yield strengths that are several times as large as those of conventional alloys, that make them attractive for a variety of applications (*3*–*5*). The mechanisms by which materials deform during mechanical milling to produce ultrafine grains are not known, although it is thought that turbulent shear processes requiring crystal rotation are operative and that disclinations contribute to this process (*6*, *7*). Similarly, the reasons for the unusual mechanical properties are not fully understood, but have been attributed to the nature of grain boundaries (*5*, *8*–*10*), the fine grain size, and/or the presence of defects such as disclinations, dislocations, and twins (*1*–*4*, *7*, *11*–*14*). We report the use of high-resolution transmission electron microscopy (HRTEM) (*15*, *16*) to directly observe the atomic structure of partial disclination dipoles in body-centered cubic (bcc) Fe that had undergone severe plastic deformation by mechanical milling.

Disclinations are special physical objects that serve as carriers of violation of rotational symmetry (*6*, *17*). They are found throughout nature and are used to describe such diverse phenomena as the arrangement of molecules in liquid crystals (*17*, *18*), the deformation behavior of metals (*6*, *7*), polarization effects and diffraction of electromagnetic waves (*19*), displacements of Earth's crust (*20*), galactic structures (*21*), misorientation in heteroepitaxial diamond films (*22*), and so forth. Disclinations in crystalline materials can alternatively be described in terms of individual line defects in the atomic structure called dislocations (*23*, *24*). It is possible to image the atomic structures of defects such as dislocations in crystalline solids by means of HRTEM (*15*, *16*). For example, HRTEM has been used to reveal the atomic structures of individual dislocations and arrays of dislocations such as grain boundaries in a variety of materials, including semiconductors and metal alloys, where their presence has a profound effect on the electro-optical and mechanical properties of the materials, respectively (*15*, *16*). HRTEM has also been used to reveal the structure and behavior of disclinations in a variety of polymeric materials at the microscopic and molecular levels (*18*, *25*). In contrast, the atomic structure of disclination defects in inorganic crystalline solids has rarely been directly observed (*22*, *26*).

The procedure of making a mechanically milled, pure Fe powder has been described in detail (*4*). In summary, commercially pure Fe powder was mechanically milled with steel balls by using a planetary ball mill for 100 hours under an Ar gas atmosphere. During this process, the Fe powder is mashed between the steel balls and undergoes severe plastic deformation at high strain rates. After the fabrication process, the bcc Fe powder had a hardness of 850 on the Vickers scale. HRTEM specimens were prepared from the Fe powder by ion milling and were examined in a JEOL JEM-4000EX microscope equipped with a UHP40H pole-piece and operating at 400 kV. The point resolution of the microscope at Scherzer defocus (−49.0 nm) is 0.18 nm, and this is sufficient to image the atomic structure of bcc Fe when it is oriented such that the κ axis in the crystal structure is parallel to the viewing direction (Fig. 1).

Figure 2A shows a HRTEM image of the mechanically milled, nanocrystalline Fe powder. The image is ~20.5 nm wide. The grain that occupies most of the figure is in a κ orientation. The hexagonal arrangement of columns of Fe atoms in this orientation are visible as white spots, as in the simulated

[1]Department of Materials Science and Engineering, University of Virginia, Charlottesville, VA 22904–4745, USA. [2]Department of Materials Science and Engineering, Kyushu University, Fukuoka, 812-8581, Japan.

*On leave from the National Institute for Materials Science, Tsukuba, 305-0047, Japan.

†To whom correspondence should be addressed. E-mail: jh9s@virginia.edu